Article

Synthesis of Highly Transparent Diblock Copolymer Vesicles via RAFT Dispersion Polymerization of 2,2,2-Trifluoroethyl Methacrylate in *n*-Alkanes

Csilla György, Matthew J. Derry, Erik J. Cornel, and Steven P. Armes*

Cite This: https://dx.doi.org/10.1021/acs.macromol.0c02646
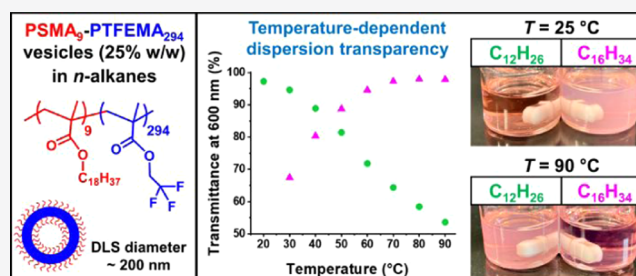
Read Online

ACCESS | Metrics & More | Article Recommendations | SI Supporting Information

ABSTRACT: RAFT dispersion polymerization of 2,2,2-trifluoroethyl methacrylate (TFEMA) is performed in *n*-dodecane at 90 °C using a relatively short poly(stearyl methacrylate) (PSMA) precursor and 2-cyano-2-propyl dithiobenzoate (CPDB). The growing insoluble poly(2,2,2-trifluoroethyl methacrylate) (PTFEMA) block results in the formation of PSMA–PTFEMA diblock copolymer nano-objects via polymerization-induced self-assembly (PISA). GPC analysis indicated narrow molecular weight distributions ($M_w/M_n \leq 1.34$) for all copolymers, with ^{19}F NMR studies indicating high TFEMA conversions ($\geq 95\%$) for all syntheses. A pseudo-phase diagram was constructed to enable reproducible targeting of pure spheres, worms, or vesicles by varying the target degree of polymerization of the PTFEMA block at 15–25% w/w solids. Nano-objects were characterized using dynamic light scattering, transmission electron microscopy, and small-angle X-ray scattering. Importantly, the near-identical refractive indices for PTFEMA (1.418) and *n*-dodecane (1.421) enable the first example of highly transparent vesicles to be prepared. The turbidity of such dispersions was examined between 20 and 90 °C. The highest transmittance (97% at 600 nm) was observed for PSMA$_9$–PTFEMA$_{294}$ vesicles (237 ± 24 nm diameter; prepared at 25% w/w solids) in *n*-dodecane at 20 °C. Interestingly, targeting the same diblock composition in *n*-hexadecane produced a vesicle dispersion with minimal turbidity at a synthesis temperature of 90 °C. This solvent enabled in situ visible absorption spectra to be recorded during the synthesis of PSMA$_{16}$–PTFEMA$_{86}$ spheres at 15% w/w solids, which allowed the relatively weak n→π* band at 515 nm assigned to the dithiobenzoate chain-ends to be monitored. Unfortunately, the premature loss of this RAFT chain-end occurred during the RAFT dispersion polymerization of TFEMA at 90 °C, so meaningful kinetic data could not be obtained. Furthermore, the dithiobenzoate chain-ends exhibited a λ_{max} shift of 8 nm relative to that of the dithiobenzoate-capped PSMA$_9$ precursor. This solvatochromic effect suggests that the problem of thermally labile dithiobenzoate chain-ends cannot be addressed by performing the TFEMA polymerization at lower temperatures.

INTRODUCTION

Block copolymer self-assembly in solution has been studied for almost six decades.[1−3] Traditionally, this has been achieved via post-polymerization processing techniques such as a solvent switch[4] or thin film rehydration.[5] However, such approaches usually only enable the synthesis of dilute colloidal dispersions of diblock copolymer nano-objects. In contrast, the development of polymerization-induced self-assembly (PISA) over the past decade or so enables the rational synthesis of diblock nano-objects of controlled size and morphology directly in the form of concentrated colloidal dispersions.[6−9] PISA simply involves growing a second block from a soluble precursor block under conditions in which the second block gradually becomes insoluble. The solvent is selected to be a poor solvent for the second block and the monomer initially acts as a co-solvent, before serving as a processing aid during the latter stages of the polymerization. Moreover, PISA is a generic concept that can

be used to prepare nano-objects in a wide range of solvents, including water, polar solvents, or non-polar solvents.[9−16]

In recent years, poly(2,2,2-trifluoroethyl methacrylate) (PTFEMA) has been utilized as a core-forming block for various aqueous and non-aqueous PISA formulations.[17−25] Semsarilar and co-workers were the first to report that choosing PTFEMA as the structure-directing block offers an opportunity to study the fate of the RAFT chain-ends during RAFT dispersion polymerization. More specifically, the refractive index of PTFEMA (1.418) is close to that of ethanol (1.361), which leads to minimal turbidity for PTFEMA-core

nanoparticles in this solvent. This enabled the living character of RAFT solution polymerization to be compared with that of RAFT dispersion polymerization by targeting the same diblock copolymer formulation and monitoring the gradual loss of RAFT chain-ends via UV spectroscopy.[17] Akpinar et al. reported the RAFT aqueous emulsion polymerization of TFEMA using poly(glycerol monomethacrylate) (PGMA) as a stabilizer block to produce a series of kinetically-trapped spheres.[19] Such nanoparticles were used as Pickering emulsifiers by Thompson et al. to produce oil-in-water nanoemulsions with relatively high stability.[21,26] Subsequently, Rymaruk and co-workers demonstrated that highly transparent *isorefractive* Pickering emulsions could be prepared by using PGMA−PTFEMA spherical nanoparticles. This is because the refractive index of water can be raised to that of PTFEMA (and *n*-dodecane) by dissolution of sufficient quantities of either glycerol or sucrose.[20] Recently, Cornel et al. reported that careful optimization of a PISA formulation (i.e., the choice of *n*-alkane and reaction temperature) enabled the rational design of an isorefractive dispersion of PTFEMA-core spherical nanoparticles using a poly(stearyl methacrylate) (PSMA) precursor. At the chosen reaction temperature (70 °C), the preferred *n*-alkane (*n*-tetradecane) had almost precisely the same refractive index as the growing PTFEMA block, which resulted in a highly transparent dispersion. This enabled the kinetics of the RAFT dispersion polymerization of TFEMA to be monitored by in situ visible absorption spectroscopy studies of the relatively weak $n \rightarrow \pi^*$ transition for the trithiocarbonate end-group at 446 nm.[23] In a related study, Smith et al. reported that highly transparent PSMA−PTFEMA spherical nanoparticles prepared in *n*-tetradecane are well suited to dynamic light scattering (DLS) experiments for nanoparticle diffusion studies, while the large electron density difference between the PTFEMA block and the solvent provided excellent contrast for X-ray scattering measurements.[24]

Herein we report the PISA synthesis of a series of PSMA_9−PTFEMA_x nano-objects via RAFT dispersion polymerization of TFEMA in *n*-dodecane at 90 °C. The use of a relatively short PSMA_9 precursor block ensured access to the full range of copolymer morphologies (i.e., spheres, worms, and vesicles). A pseudo-phase diagram has been constructed for this PISA formulation by targeting PTFEMA degrees of polymerizations (DPs) ranging from 20 to 300 at 15–25% w/w solids. Copolymer morphologies were initially assigned on the basis of DLS and transmission electron microscopy (TEM) studies and subsequently confirmed by small-angle X-ray scattering (SAXS) analysis. *In particular, this PISA formulation provides the first example of highly transparent block copolymer vesicles owing to the close match between the refractive indices of PTFEMA and n-dodecane at 20 °C.* Moreover, the variation in refractive index with temperature enables minimization of the turbidity of PSMA_9−PTFEMA_x nanoparticle dispersions at an elevated temperature in either *n*-tetradecane or *n*-hexadecane. Such formulations enable in situ visible absorption spectroscopy studies to be performed during the RAFT dispersion polymerization of TFEMA when using a dithiobenzoate RAFT agent to target PSMA_16−PTFEMA_86 spheres at 15% w/w solids in *n*-hexadecane at 90 °C.

■ EXPERIMENTAL SECTION

Materials. Stearyl methacrylate (SMA) was purchased from Santa Cruz Biotechnology, Inc. (USA) and was used as received. 2,2,2-

Trifluoroethyl methacrylate (TFEMA) was purchased from Fluorochem Ltd. (U.K.) and was used without further purification. 2-Cyano-2-propyl dithiobenzoate (CPDB), CDCl_3, *n*-dodecane, *n*-hexadecane, and *n*-tetradecane were purchased from Merck (U.K.). 2,2′-Azoisobutyronitrile (AIBN) was obtained from Molekula (U.K.), and *tert*-butyl peroxy-2-ethylhexanoate (T21s) was purchased from AkzoNobel (The Netherlands). CD_2Cl_2 was purchased from Goss Scientific (U.K.). Tetrahydrofuran and *n*-heptane were obtained from VWR Chemicals (U.K.). Ethanol and toluene were purchased from Fisher Scientific (U.K.).

Synthesis of Poly(stearyl methacrylate) (PSMA) Stabilizer Block via RAFT Solution Polymerization in Toluene. PSMA_9 and PSMA_16 stabilizer blocks were prepared by following a recently reported synthesis protocol.[27,28] The synthesis of PSMA_9 was conducted as follows: SMA (30.0 g; 88.6 mmol), CPDB (3.92 g; 17.7 mmol; target DP = 5.0), AIBN (582 mg; 3.55 mmol; CPDB/AIBN molar ratio = 5.0), and toluene (34.5 g) were weighed into a 250 mL round-bottomed flask. The sealed reaction vessel was purged with nitrogen for 30 min and placed in a preheated oil bath at 70 °C with stirring for 4 h. The ensuing SMA polymerization was then quenched by exposing the reaction solution to air and cooling to room temperature. A final SMA conversion of 78% was determined by ^{1}H NMR spectroscopy. To remove residual monomer, the crude polymer was purified by three consecutive precipitations into a 10-fold excess of ethanol. The mean DP of the stabilizer block was calculated to be 9 using ^{1}H NMR analysis by comparing the aromatic protons of the dithiobenzoate end-group at 6.8−8.0 ppm to the two oxymethylene protons of PSMA at 3.6−4.0 ppm. THF GPC analysis of PSMA_9 using a UV detector (set at λ = 260 nm) and a series of near-monodisperse polystyrene standards indicated an M_n of 2700 g mol^{-1} and an M_w/M_n of 1.22. GPC analysis of PSMA_16 gave M_n = 5500 g mol^{-1} and M_w/M_n = 1.16.

Synthesis of Poly(stearyl methacrylate)-poly(2,2,2-trifluoroethyl methacrylate) (PSMA−PTFEMA) Diblock Copolymer Nanoparticles via RAFT Dispersion Polymerization of TFEMA in *n*-Dodecane. A typical example is the PISA synthesis of PSMA_9−PTFEMA_294 diblock copolymer vesicles at 25% w/w solids, which was conducted as follows: PSMA_9 macro-CTA (0.05 g; 15.30 μmol), T21s initiator (1.10 mg; 5.06 μmol; 10.0% v/v in *n*-dodecane) and *n*-dodecane (2.47 g) were weighed into a sample vial and purged with nitrogen for 30 min. TFEMA monomer (0.65 mL; 4.59 mmol; target DP = 300) was degassed separately and then added to the reaction mixture via syringe. The vial was immersed in a preheated oil bath at 90 °C, and the reaction mixture was magnetically stirred for 17 h. ^{19}F NMR analysis indicated 98% TFEMA monomer conversion by comparing the integrated monomer triplet signal at −74.0 ppm to the integrated polymer signal at −73.5 ppm (see Figure S1). THF GPC analysis indicated an M_n of 26 500 g mol^{-1} and an M_w/M_n of 1.31. PSMA_9−PTFEMA_294 diblock copolymer vesicles were also prepared at 25% w/w solids following the same protocol using either *n*-tetradecane or *n*-hexadecane instead of *n*-dodecane. To construct a pseudo-phase diagram for PSMA_9−PTFEMA_x nano-objects prepared in *n*-dodecane, a range of diblock copolymer compositions were targeted between 15 and 25% w/w solids by adjusting the total volume of the dispersion to 2.0 mL and varying the TFEMA/PSMA_9 molar ratio accordingly.

NMR Spectroscopy. ^{1}H NMR spectra were recorded in either CD_2Cl_2 or CDCl_3 using a 400 MHz Bruker Avance spectrometer. Typically, 64 scans were averaged per spectrum. ^{19}F NMR spectra were recorded in either CD_2Cl_2 or CDCl_3 using a 400 MHz Bruker Avance spectrometer. Typically, 16 scans were averaged per spectrum.

Gel Permeation Chromatography (GPC). Molecular weight distributions (MWDs) were assessed by GPC using THF eluent. The THF GPC system was equipped with two 5 μm (30 cm) Mixed C columns and a WellChrom K-2301 refractive index detector operating at 950 ± 30 nm. The THF mobile phase contained 2.0% v/v triethylamine and 0.05% w/v butylhydroxytoluene (BHT), and the flow rate was fixed at 1.0 mL min^{-1}. A series of nine near-monodisperse polystyrene standards (M_p values ranging from 580 to

550 100 g mol^{-1}) were used for column calibration in combination with a UV detector operating at a fixed wavelength of 260 nm.

Dynamic Light Scattering (DLS). DLS studies were performed using a Zetasizer Nano ZS instrument (Malvern Instruments, U.K.) at a fixed scattering angle of 173°. Copolymer dispersions were diluted in *n*-heptane (0.10% w/w) prior to light scattering studies at 25 °C. The intensity-average diameter and polydispersity of the diblock copolymer nanoparticles were calculated by cumulant analysis of the experimental correlation function using Dispersion Technology Software version 6.20. Data were averaged over 10 runs each of 30 seconds duration. It is emphasized that DLS assumes a spherical morphology. Thus, the DLS diameter determined for highly anisotropic particles such as worms is a "sphere-equivalent" value that is equal to neither the worm length nor the worm width.

Transmission Electron Microscopy (TEM). TEM studies were conducted using a Philips CM 100 instrument operating at 100 kV and equipped with a Gatan 1 k CCD camera. A single droplet of a 0.10% w/w diblock copolymer dispersion was placed onto a carbon-coated copper grid using a pipet and allowed to dry, prior to exposure to ruthenium(VIII) oxide vapor for 7 min at 20 °C.[29] This heavy metal compound acted as a positive stain for the core-forming PTFEMA block to improve contrast. The ruthenium(VIII) oxide was prepared as follows: ruthenium(IV) oxide (0.30 g) was added to water (50 g) to form a black slurry; the addition of sodium periodate (2.0 g) with continuous stirring produced a yellow solution of ruthenium(VIII) oxide within 1 min at 20 °C.

Small-Angle X-ray Scattering (SAXS). SAXS patterns were collected at a synchrotron source (Diamond Light Source, station I22, Didcot, UK; experiment number SM19852) using a monochromatic X-ray radiation (wavelength $\lambda = 0.100$ nm, with q ranging from 0.015 to 1.8 nm^{-1}, where $q = 4\pi \sin \theta / \lambda$ is the length of the scattering vector and θ is the one-half of the scattering angle) and a two-dimensional (2D) Pilatus 2M pixel detector (Dectris, Switzerland). A glass capillary of 2 mm diameter was used as a sample holder. Scattering data were reduced using standard routines from the beamline[30] and were further analyzed using Irena SAS macros for Igor Pro.[31]
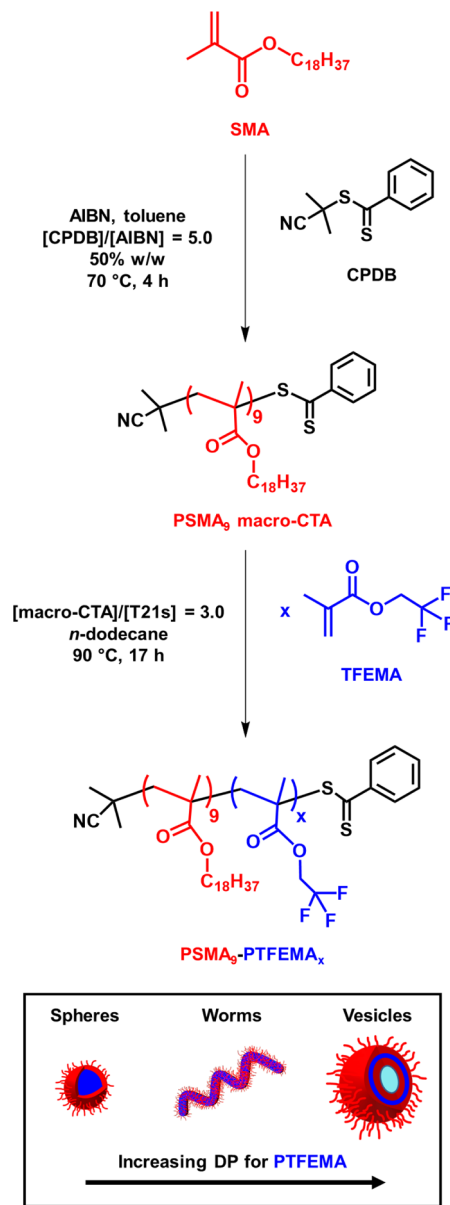
UV−Visible Spectroscopy Studies of Vesicle Dispersions. The transmittance of vesicle dispersions prepared at 25% w/w solids in various *n*-alkanes was studied using a PC-controlled UV-1800 spectrophotometer equipped with a 10 mm pathlength quartz cell. Spectra were recorded between 200 and 800 nm from 20 °C to 90 °C by increasing the temperature at 10 °C intervals. The transmittance was determined at $\lambda = 600$ nm and corrected by the pure solvent transmittance at each temperature determined prior to analysis of the vesicle dispersions. This wavelength was chosen to avoid the absorption bands associated with the dithiobenzoate chain-ends at approximately 300 and 507 nm.

In Situ UV−Visible Spectroscopy Studies of the Synthesis of PSMA$_{16}$−PTFEMA$_{90}$ Spheres in *n*-Hexadecane. This experiment was conducted using an Agilent Cary 60 spectrometer equipped with a Hellma all-quartz UV−visible immersion probe, 1.8 m fiber optic cables, and SMA 905 connectors. This probe has a wavelength range of 190−1100 nm, can operate between 5 and 150 °C, and has a 10 mm pathlength. The baseline for pure *n*-hexadecane was recorded at 90 °C prior to the in situ experiment. During the PISA synthesis conducted at 90 °C, the spectra were recorded between 200 and 800 nm at a spectral resolution of ±3 nm using a scan rate of 1800 nm min^{-1} at 1 min intervals for the first 20 min of the polymerization and then at 2 min intervals for the remaining 880 min. In a final experiment, the spectral resolution was adjusted to ±1 nm.

■ RESULTS AND DISCUSSION

Synthesis of PSMA Stabilizer Precursors. Two PSMA precursors with mean DPs of either 9 (target DP = 5) or 16 (target DP = 20) were synthesized via RAFT solution polymerization of SMA in toluene at 70 °C using a CPDB RAFT agent, as shown in Scheme 1. To preserve the dithiobenzoate end-groups (i.e., avoid monomer-starved conditions), the polymerization was quenched after 4 h in

Scheme 1. Synthesis of Poly(stearyl methacrylate) (PSMA$_9$) Macro-CTA via RAFT Solution Polymerization in Toluene Using 2-Cyano-2-propyl Benzodithioate (CPDB) at 70 °C, Followed by the RAFT Dispersion Polymerization of 2,2,2-Trifluoroethyl Methacrylate (TFEMA) in *n*-Dodecane at 90 °C

the case of PSMA$_9$ and after 5 h for PSMA$_{16}$.[32] ^{1}H NMR spectroscopy studies indicated SMA conversions of 78% (PSMA$_9$) and 60% (PSMA$_{16}$). Relatively good RAFT control ($M_w/M_n \leq 1.22$) was confirmed by THF GPC analysis in both cases.

Kinetic Studies of the RAFT Dispersion Polymerization of TFEMA in *n*-Dodecane. Kinetic data was obtained for the RAFT dispersion polymerization of TFEMA at 90 °C when targeting PSMA$_9$−PTFEMA$_{200}$ vesicles at 20% w/w solids in *n*-dodecane. The reaction mixture was periodically sampled, and each aliquot was diluted with CD$_2$Cl$_2$ prior to ^{19}F NMR spectroscopy analysis, which enabled excellent discrimination between the TFEMA monomer and PTFEMA signals. The corresponding semi-

logarithmic plot indicates three distinct linear regimes (see Figure 1a). Cornel et al. recently reported similar observations
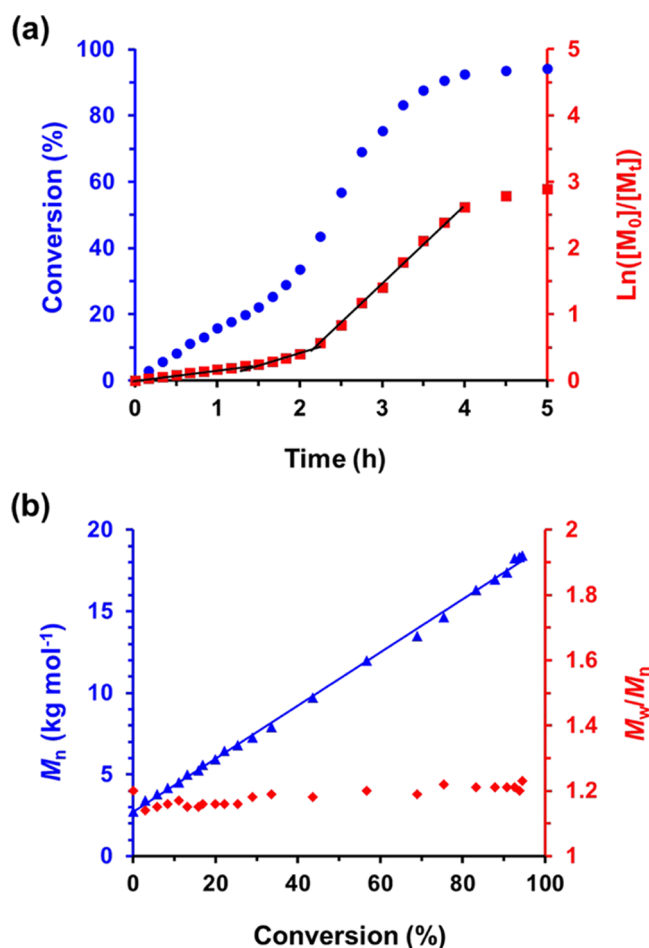

Figure 1. (a) Conversion vs time curve (blue circles) and the corresponding $\ln([M_0]/[M_t])$ vs time plot (red squares) for the RAFT dispersion polymerization of TFEMA at 90 °C targeting $PSMA_9-PTFEMA_{200}$ diblock copolymer vesicles at 20% w/w solids in n-dodecane. (b) Evolution of M_n (blue triangles, vs polystyrene calibration standards) and M_w/M_n (red diamonds) with TFEMA monomer conversion for this PISA formulation.

for the synthesis of $PSMA_{12}-PTFEMA_{98}$ spheres in n-tetradecane.[23] The initial solution polymerization proceeds relatively slowly, and then an approximate two-fold rate enhancement is observed after 1.5 h. This marks the onset of micellar nucleation for this PISA formulation[23,33−35] and corresponds to the point at which the PTFEMA block becomes insoluble in the reaction mixture, resulting in the formation of spherical micelles by in situ self-assembly. This occurs at approximately 22% TFEMA conversion, for which the theoretical PTFEMA DP is calculated to be around 45. A subsequent four-fold rate enhancement occurs after 2 h, which corresponds to ∼34% TFEMA conversion and a PTFEMA DP of approximately 67. First-order kinetics were observed thereafter up to 93% TFEMA conversion, whereupon a slower rate of polymerization occurs under monomer-starved conditions. More than 95% TFEMA conversion was achieved within 5 h at 90 °C. THF GPC analysis indicates a linear evolution of M_n with conversion (see Figure 1b) and relatively low dispersities throughout the polymerization ($M_w/M_n \leq$

1.23), which is consistent with the pseudo-living character expected for a RAFT polymerization.[36−38]

RAFT Dispersion Polymerization of TFEMA in n-Dodecane. The chain extension of $PSMA_{13}$ and $PSMA_{18}$ stabilizer blocks via RAFT dispersion polymerization of glycidyl methacrylate in mineral oil was studied by Docherty et al.[34] For this prior PISA formulation, only kinetically-trapped spheres could be obtained because the steric stabilizer block was sufficiently long to prevent 1D sphere−sphere fusion. However, we have subsequently shown that using a shorter stabilizer block ($PSMA_9$) provides access to the full range of copolymer morphologies (i.e., spheres, worms, or vesicles).[27,28] Herein the RAFT dispersion polymerization of TFEMA was examined using such a $PSMA_9$ macro-CTA in n-dodecane at 90 °C.

Semsarilar et al. reported that GPC analysis of PTFEMA-based diblock copolymers can be problematic because of the relatively low refractive index of PTFEMA (1.418) compared to that of most other methacrylates (1.491−1.596).[17] This means that a GPC refractive index detector tends to underestimate the signal arising from the semifluorinated PTFEMA block relative to the other (nonfluorinated) block. This typically produces a bimodal molecular weight distribution, which at first sight suggests significant contamination of the diblock copolymer by the non-fluorinated macro-CTA.[17] However, this is simply an experimental artifact owing to the mismatched refractive indices: the true level of macro-CTA contamination is significantly lower. Fortunately, the dithiobenzoate-capped diblock copolymer chains formed in the present study enable a UV detector to be used for GPC analysis. Chromatograms for four $PSMA_9-PTFEMA_{38-291}$ diblock copolymers prepared at 20% w/w solids recorded using a UV detector at a fixed wavelength of 260 nm are shown in Figure 2a, along with the corresponding chromatogram recorded for the $PSMA_9$ precursor. The latter has a relatively low dispersity ($M_w/M_n = 1.22$), and oligomers are partially resolved at longer retention times. Each of the four diblock copolymers exhibits a unimodal and reasonably narrow molecular weight distribution ($M_w/M_n \leq 1.31$). In contrast, GPC analysis of the $PSMA_9-PTFEMA_{291}$ diblock copolymer using a refractive index detector indicated a somewhat broader molecular weight distribution ($M_w/M_n = 1.49$) owing to the appearance of a low molecular weight shoulder, which is assigned to the (exaggerated) presence of the contaminating $PSMA_9$ precursor (see Figure S2). On the basis of these preliminary findings, UV GPC was preferred for the analysis of the $PSMA_9-PTFEMA_x$ diblock copolymers reported in this study.

UV GPC data obtained for a series of $PSMA_9-PTFEMA_x$ nanoparticles prepared at 20% w/w solids are shown in Figure 2b. There is a linear correlation between the GPC M_n data and the actual PTFEMA DP (after correcting for the TFEMA conversion) when the latter is systematically varied from 19 to 291. Reasonably narrow molecular weight distributions ($M_w/M_n \leq 1.31$) were obtained for mean PTFEMA DPs up to 291. This is comparable to GPC data reported by Derry et al. and Docherty et al. for similar RAFT dispersion polymerization formulations conducted in mineral oil.[27,32,34,35] The broader molecular weight distributions that are observed when targeting higher DPs are most likely the result of chain transfer to polymer.[39] The pendent methylene group in the TFEMA repeat units is expected to be particularly susceptible
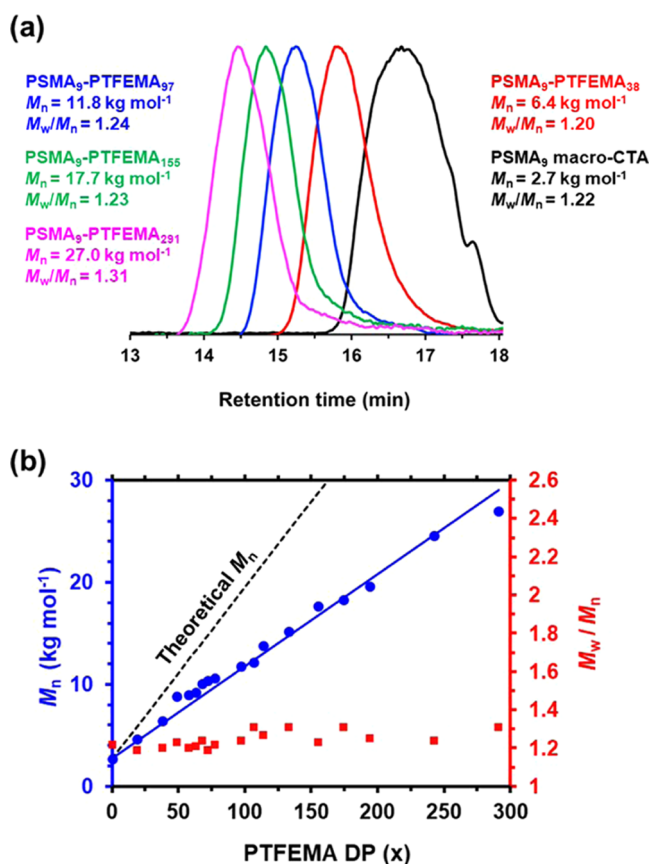
Figure 2. (a) Gel permeation chromatograms (vs a series of near-monodisperse polystyrene calibration standards using a UV detector set at 260 nm) obtained for the $PSMA_9$ precursor (prepared in toluene at 50% w/w solids at 70 °C) and a series of four $PSMA_9-PTFEMA_x$ diblock copolymers prepared by RAFT dispersion polymerization of TFEMA at 90 °C at 20% w/w solids, where the mean DPs of the core-forming block were 38, 97, 155, or 291, respectively. (b) Correlation between GPC M_n (blue circles, vs PS calibration standards) and actual PTFEMA DP (as determined by ^{19}F NMR) for a larger series of $PSMA_9-PTFEMA_x$ diblock copolymers at 20% w/w solids. The corresponding GPC M_w/M_n (red squares) are also shown.

to this side reaction owing to the highly electronegative nature of the three neighboring fluorine atoms.

A pseudo-phase diagram was constructed to aid the reproducible targeting of pure spheres, worms, and vesicles in *n*-dodecane (see Figure 3). A series of $PSMA_9-PTFEMA_x$ copolymers were produced by varying the target DP for PTFEMA between 20 and 300 for formulations conducted at 15, 20, or 25% w/w solids respectively, (see Tables S1 and S2). $PSMA_9-PTFEMA_{38}$ spheres could be produced at all copolymer concentrations examined, with *z*-average diameters of 18−21 nm (DLS polydispersity (or PDI) ≤ 0.33) as judged by DLS. Unlike $PSMA_9-PHPMA_x$ formulations[28] previously examined in mineral oil, a relatively broad worm phase was observed with well-defined worms being obtained at a copolymer concentration as low as 15% w/w. A digital photograph recorded for $PSMA_9-PTFEMA_{63}$ worms prepared at 20% w/w solids confirms the relatively high transparency of such free-standing gels (see Figure S3). However, similar findings have been reported for many other PISA formulations in various solvents because the mean worm width is usually so small that such nano-objects do not scatter light particularly
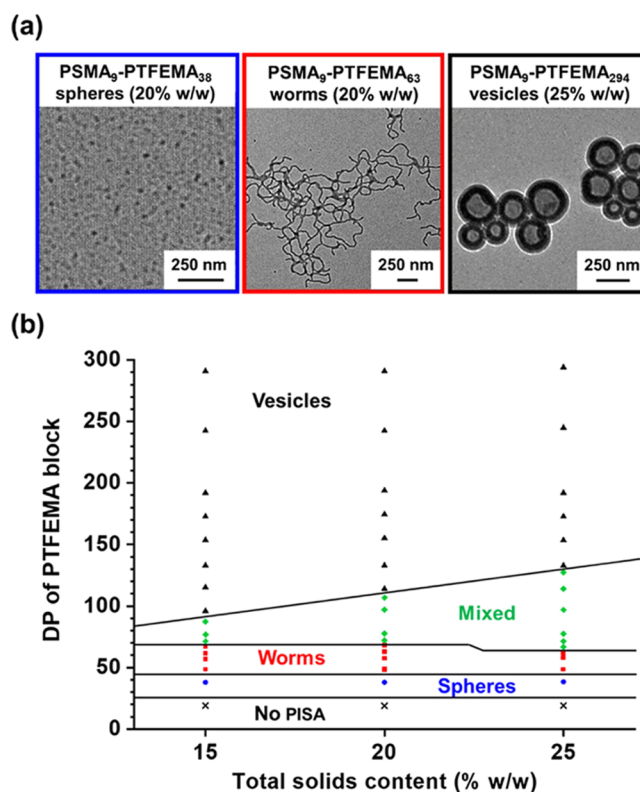

Figure 3. (a) Representative TEM images obtained for $PSMA_9-PTFEMA_{38}$ spheres, $PSMA_9-PTFEMA_{63}$ worms, and $PSMA_9-PTFEMA_{294}$ vesicles prepared at 20, 20, and 25% w/w solids, respectively. (b) Pseudo-phase diagram constructed for $PSMA_9-PTFEMA_x$ diblock copolymer nano-objects prepared by RAFT dispersion polymerization of TFEMA in *n*-dodecane using a $PSMA_9$ macro-CTA and T21s initiator at 90 °C ($[PSMA_9]/[T21s]$ molar ratio = 3.0). Green diamonds correspond to a mixed phase comprising worms and vesicles (plus a minor population of spheres in some cases).

strongly.[27,40−44] In contrast, the formation of vesicles invariably leads highly turbid dispersions, regardless of whether such dispersions are prepared directly via PISA or indirectly via post-polymerization processing.[27,40,42,45−50] Indeed, we are not aware of any literature reports of the synthesis of highly transparent vesicle dispersions. However, all $PSMA_9-PTFEMA_x$ vesicles obtained at up to 25% w/w solids in *n*-dodecane by targeting a PTFEMA DP (x) of 140−300 proved to be highly transparent at 20 °C.

Transmittance vs wavelength plots recorded at 25 °C for 0.50% w/w dispersions of $PSMA_9-PTFEMA_{294}$ vesicles (DLS diameter = 237 nm, PDI = 0.10) and $PSMA_9-PHPMA_{294}$ vesicles (DLS diameter = 175 nm, PDI = 0.03) are compared in Figure 4. In both cases, the vesicles were originally prepared at 25% w/w in *n*-dodecane and subsequently diluted to 0.50% w/w using the same solvent. The $PSMA_9-PHPMA_{294}$ vesicles form a *relatively turbid* dispersion (e.g., 31% transmittance at λ = 600 nm) owing to the refractive index difference between the PHPMA block (∼1.51 at 20 °C) and *n*-dodecane (1.421 at 20 °C), which leads to light scattering. In contrast, the *larger* $PSMA_9-PTFEMA_{294}$ vesicles form a *highly transparent* dispersion (e.g., more than 99% transmittance at λ = 600 nm) because the PTFEMA block (refractive index = 1.418 at 20 °C) is almost perfectly isorefractive with the same solvent at 20−25 °C.

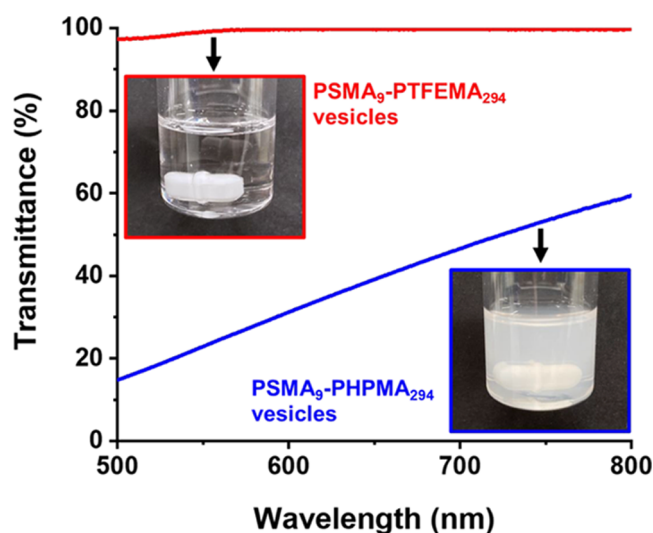**Figure 4.** Transmittance vs wavelength plots recorded at 25 °C for 0.50% w/w dispersions of PSMA$_9$−PTFEMA$_{294}$ (red data) and PSMA$_9$−PHPMA$_{294}$ (blue data) vesicles in *n*-dodecane. These vesicles were originally prepared at 25% w/w in *n*-dodecane by RAFT dispersion polymerization of either TFEMA or HPMA, respectively. Insets: digital photographs recorded for the 0.50% w/w dispersions at 25 °C to illustrate their differing turbidity.

Small-angle X-ray scattering (SAXS) patterns were recorded for 1.0% w/w dispersions of selected PSMA$_9$−PTFEMA$_x$ nano-objects originally synthesized at 20% w/w in *n*-dodecane (see Figure 5). SAXS offers important advantages over TEM
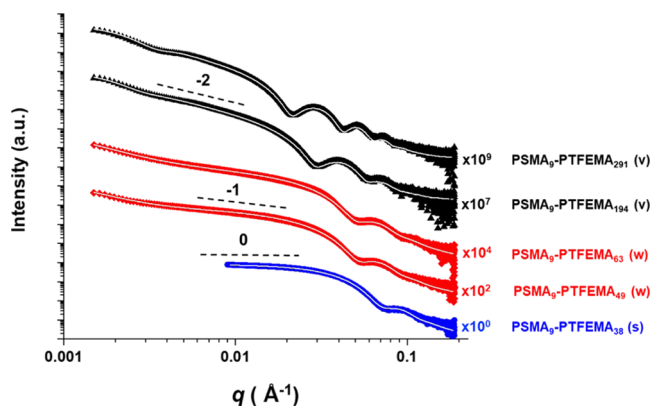

Figure 5. Small-angle X-ray scattering (SAXS) patterns and corresponding data fits (white lines) for 1.0% w/w dispersions of PSMA$_9$−PTFEMA$_x$ spheres, worms, and vesicles in *n*-dodecane at 20 °C. These nano-objects were initially synthesized at 20% w/w solids. Black dashed lines indicate gradients of 0, −1, and −2 for guidance to the eye.

and DLS. Data are averaged over millions of nanoparticles in their native dispersed state, unlike the hundreds of dried nano-objects typically analyzed by TEM. Moreover, SAXS enables much more rigorous analysis of highly anisotropic nano-objects such as worms than DLS, not least because the latter technique assumes a spherical morphology. Similarly, SAXS provides additional structural information for vesicles such as the mean membrane thickness. In the first instance, SAXS analysis can be used to corroborate the pseudo-phase diagram shown in Figure 3b, for which morphology assignments were based on TEM studies. Indeed, preliminary inspection of the low *q* region of

the SAXS patterns recorded for each dispersion indicated the same morphology as that suggested by TEM. More specifically, gradients of approximately 0, −1, and −2 were observed for spheres, worms, and vesicles, respectively (see Figure 5). These initial observations were further validated by obtaining satisfactory fits to these SAXS patterns when using established spherical micelle,[51] worm-like micelle,[51] or vesicle[52] models. These data fits also provided volume-average nanoparticle dimensions and the mean number of copolymer chains per nano-object, otherwise known as the aggregation number (N_{agg}), as summarized in Table S3. For example, PSMA$_9$−PTFEMA$_{38}$ spheres have an overall diameter (D_{sphere}) of 14.6 ± 1.7 nm, with an N_{agg} of 110. For PSMA$_9$−PTFEMA$_{49}$ and PSMA$_9$−PTFEMA$_{63}$ worms, the overall worm thicknesses (T_{worm}) were 15.8 ± 2.0 and 16.4 ± 2.1 nm, respectively, with slightly thicker worms being formed as the PTFEMA DP (x) was increased, as expected. Moreover, the mean worm contour lengths (L_{worm}) were comparable (905 vs 1040 nm, respectively) and similar N_{agg} values (13 700 vs 13 400) were obtained. Similarly, the vesicle membrane thickness ($T_{membrane}$) increased from 20.6 ± 4.4 to 28.8 ± 4.4 nm on increasing x from 194 to 291, but the overall vesicle diameter ($D_{vesicle}$) remained relatively constant (195 ± 66 and 190 ± 48 nm, respectively). This apparent "inward growth" of vesicles on increasing the membrane-forming block DP is consistent with observations previously reported by Warren et al.[53] and Derry et al.[32] for aqueous and non-polar PISA formulations, respectively. Interestingly, N_{agg} was reduced by ~19% from 50 700 to 41 100 on increasing x from 200 to 300, which suggests that copolymer chain rearrangement/reorganization may well occur during the vesicle growth phase for this PISA formulation.[53]

Transmittance of PSMA$_9$−PTFEMA$_{294}$ Diblock Copolymer Vesicles Synthesized at 25% w/w Solids in Various *n*-Alkanes. Recently, we reported the synthesis of highly transparent PSMA$_{12}$−PTFEMA$_{98}$ spherical nanoparticles via RAFT dispersion polymerization of TFEMA in *n*-tetradecane at 70 °C. The minimal turbidity of this PISA formulation enabled the kinetics of the TFEMA polymerization to be monitored in situ using visible absorption spectroscopy.[23] Subsequently, we demonstrated that selecting *n*-dodecane rather than *n*-tetradecane enabled high transmittance to be achieved for PSMA$_{32}$−PTFEMA$_{490}$ spheres at 30 °C owing to the differing temperature dependence of the refractive index for the former solvent compared to that of the PTFEMA core-forming block.[23] Herein we extend this approach to present *various examples of highly transparent vesicles*. Block copolymer vesicles are invariably obtained as highly turbid dispersions[27,40,42,45,46,48] because their relatively large particle size scatters visible light much more strongly than that of spherical nanoparticles. Since *n*-dodecane (1.421 at 20 °C), *n*-tetradecane (1.429 at 20 °C), and *n*-hexadecane (1.434 at 20 °C) have similar refractive indices to PTFEMA (1.418 at 20 °C), using such *n*-alkanes as solvents for the synthesis of PSMA$_9$−PTFEMA$_x$ vesicles enables such light scattering to be minimized. Accordingly, PSMA$_9$−PTFEMA$_{294}$ vesicles were synthesized at 25% w/w solids in *n*-dodecane (DLS diameter = 237 nm, PDI = 0.10), *n*-tetradecane (DLS diameter = 209 nm, PDI = 0.06), and *n*-hexadecane (DLS diameter = 193 nm, PDI = 0.03). The transmittance (λ = 600 nm) of the resulting vesicle dispersions was determined at 10 °C intervals between 20 and 90 °C when using either *n*-dodecane (see Figure S4) or *n*-tetradecane. However, a slightly narrower temperature range

was preferred for *n*-hexadecane owing to the relatively high melting point (18 °C) of this solvent. In principle, if the same PSMA$_9$−PTFEMA$_{294}$ vesicles are synthesized at a fixed copolymer concentration, the turbidity of the dispersion should simply depend on the refractive index difference obtained between the PTFEMA core and the *n*-alkane at any given temperature. Hence the highest transmittance is observed at the temperature where these two refractive indices are (almost) identical.[23] In Figure 6, this isorefractive temperature was determined to be 20 °C for vesicles synthesized in *n*-dodecane and either 50 or 90 °C when they were prepared in *n*-tetradecane or *n*-hexadecane, respectively.

In Situ Visible Absorption Spectroscopy Study during the Synthesis of PSMA$_{16}$−PTFEMA$_{86}$ Spherical Nanoparticles in *n*-Hexadecane. To record high-quality visible absorption spectra during the RAFT dispersion polymerization of TFEMA, three criteria must be fulfilled.[23] First, nanoparticle scattering must be minimized (preferably eliminated) by obtaining an isorefractive dispersion at the reaction temperature.[23] For the current PISA formulation, this can be achieved by employing *n*-hexadecane as a solvent at 90 °C (see Figure 6) while targeting relatively small PSMA$_{16}$−PTFEMA$_{86}$ spherical nanoparticles (in this case, DLS studies indicate a *z*-average diameter of 26 nm and a PDI of 0.05). Ideally, the absorbance of the initial and final reaction mixtures should remain below unity to ensure that the Beer−Lambert law remains valid. The former can be achieved by utilizing a longer stabilizer block (PSMA$_{16}$) to produce kinetically-trapped spheres, while the latter requires the copolymer concentration to be reduced to 15% w/w solids. In principle, the kinetics of polymerization can be monitored by focusing on the relatively weak absorption band associated with the n → π* transition for *dithiobenzoate* chain-ends at 515 nm in preference to the much stronger π → π* transition that occurs at approximately 300 nm.[23] The final requirement is that the RAFT chain-ends must remain stable throughout the duration of the TFEMA polymerization.

Cornel et al. recorded high-quality visible absorption spectra during the synthesis of PSMA$_{12}$−PTFEMA$_{98}$ spheres at 30% w/w solids in *n*-tetradecane using a *trithiocarbonate*-based RAFT agent at λ_{max} = 446 nm.[23] In this case, the corresponding absorbance vs time plot suggested that such chain-ends remained stable for at least 2 h under monomer-starved conditions (96% TFEMA conversion).[23] Thus the observed increase in absorbance could be directly related to the volumetric contraction of the reaction mixture that occurs on converting TFEMA monomer (ρ = 1.18 g cm^{-3}) into PTFEMA (ρ = 1.47 g cm^{-3}). This dilatometric effect enables the kinetics of the TFEMA polymerization to be monitored.[54] The question to be addressed in the present study is whether the same approach can be used to study the kinetics of TFEMA polymerization for a similar PISA formulation when using a *dithiobenzoate*-based RAFT agent.

An absorbance vs time plot recorded during the synthesis of PSMA$_{16}$−PTFEMA$_{86}$ spheres at 15% w/w solids using 2-cyano-2-propyl dithiobenzoate (CPDB) at 90 °C in *n*-tetradecane is shown in Figure 7a. For comparison, kinetic data obtained for precisely the same PISA formulation using ^{19}F NMR spectroscopy are shown in Figure 7b. If it is assumed that the dithiobenzoate chain-ends remain stable for the duration of the TFEMA polymerization, then the absorbance vs time data suggests that this reaction is complete within approximately 1 h. Moreover, a plateau region is observed at
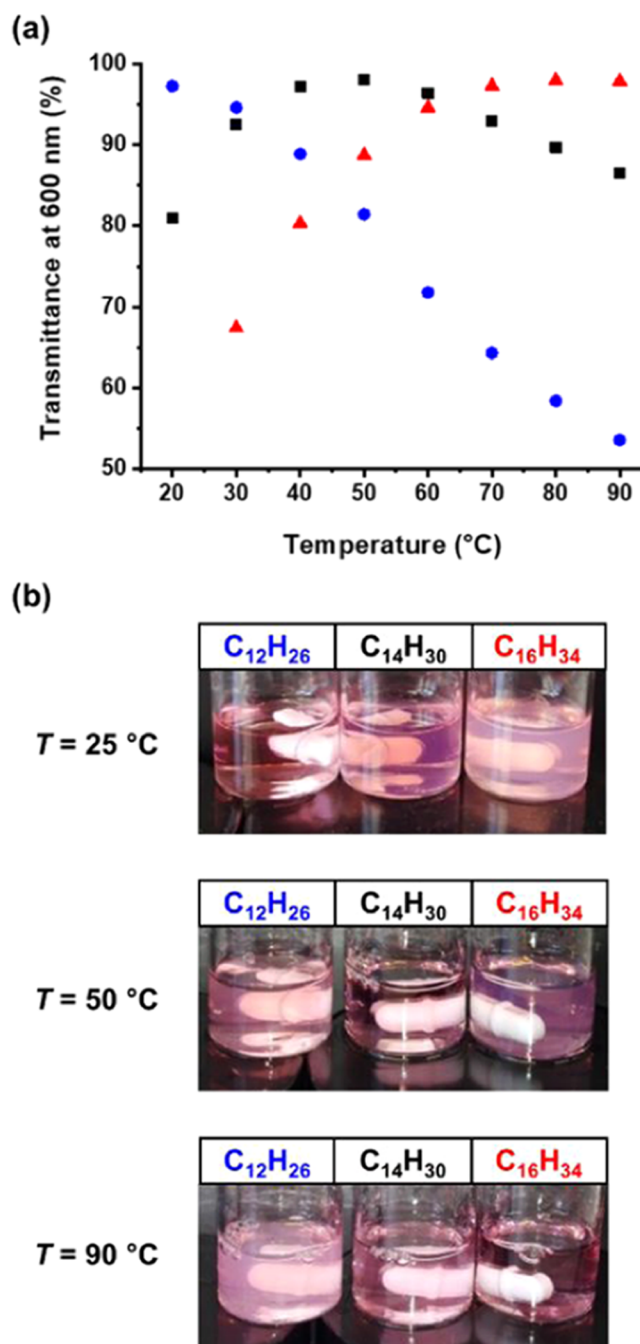

Figure 6. (a) Transmittance (λ = 600 nm) vs temperature plots recorded for PSMA$_9$−PTFEMA$_{294}$ vesicles prepared by RAFT dispersion polymerization of TFEMA at 25% w/w solids in *n*-dodecane (blue circles), *n*-tetradecane (black squares), and *n*-hexadecane (red triangles), respectively. (b) Digital photographs recorded for these three 25% w/w vesicle dispersions at 25, 50, and 90 °C to illustrate their difference in visual appearance. The most transparent dispersions are obtained in *n*-dodecane ($C_{12}H_{26}$) at 20 °C, in *n*-tetradecane ($C_{14}H_{30}$) at 50 °C, and in *n*-hexadecane ($C_{16}H_{34}$) at 90 °C. These observations informed our subsequent in situ visible absorption spectroscopy studies.

longer reaction times, which is similar to that reported by Cornel et al.[23] However, the ^{19}F NMR kinetic data indicate that only approximately 41% TFEMA conversion is achieved within the first 60 min. Indeed, 94% TFEMA conversion required a reaction time of around 3 h, whereas a gradual
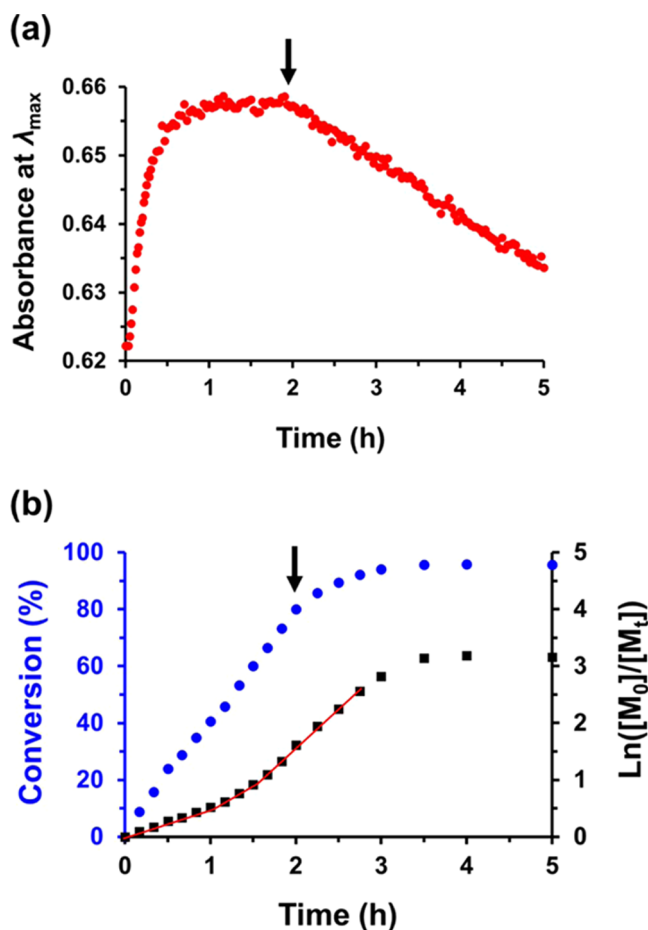
Figure 7. Synthesis of PSMA$_{16}$−PTFEMA$_{86}$ spherical nanoparticles at 15% w/w solids in *n*-hexadecane at 90 °C: (a) absorbance vs time curve and (b) conversion vs time curve (blue circles) and corresponding $\ln([M_0]/[M_t])$ vs time plot (black squares). These data confirm that the dithiobenzoate chain-ends do not remain stable on the time scale required for the TFEMA polymerization under such conditions. Instead, their gradual loss is observed within 2 h, which corresponds to a TFEMA conversion of only around 80%. Thus, the kinetics of polymerization for this particular PISA formulation cannot be monitored by visible absorption spectroscopy.

reduction in absorbance is observed after 2 h, implying the premature loss of dithiobenzoate chain-ends. Finally, it is noteworthy that both experiments produced essentially the same copolymer chains as judged by GPC (see Table S4), while the formation of relatively small spheres in both cases was confirmed by TEM and DLS analysis (see Figure S5).

It is well known that RAFT end-groups are prone to thermal degradation. Indeed, thermolysis can be used to remove such organosulfur functionality from various vinyl polymers in a post-polymerization derivatization step.[55−59] The chain-end stability depends on the monomer type, the precise chemical structure of the RAFT agent, and the reaction conditions. The thermal decomposition of dithioesters such as cumyl dithiobenzoate (CDB) at 90−120 °C and its effect on the polymerization of styrene or methyl methacrylate was studied by both Liu et al.[60] and Xu and co-workers.[61] Nejad et al. reported the in situ degradation of 4-cyanopentanoic acid-4-dithiobenzoate (CPADB) during the synthesis of poly-(methacrylic acid) and poly(methyl methacrylate) chains via RAFT solution polymerization at 80 °C in either 1,4-dioxane

or toluene, leading to the formation of dithiobenzoic acid (DTBA) as a side product.[62] Furthermore, Zhou et al. observed the thermal decomposition of CPDB in *tert*-butylbenzene at 60 °C and sought to explain such degradation in terms of the molecular structure of this RAFT agent.[63]

To examine whether the dithiobenzoate chain-ends were intrinsically unstable, the absorbance of a 4.4% w/w solution of the PSMA$_{16}$ macro-CTA in *n*-hexadecane ([PSMA$_{16}$] = 6.2 mmol dm^{-3} = 35 g dm^{-3}; this concentration corresponds to that used in the PISA formulation investigated herein) was monitored over time in an inert atmosphere at 90 °C using in situ visible absorption spectroscopy. The gradual reduction in absorbance that is observed during this experiment (see Figure S6) suggests that the premature loss of dithiobenzoate chain-ends may well occur during the early stages of the TFEMA polymerization. Moreover, the actual DP of the PTFEMA block in the final PSMA$_9$−PTFEMA$_x$ nano-objects is likely to be somewhat higher than that originally targeted.

Cornel et al. demonstrated that the absorbance vs time data recorded during the synthesis of PSMA$_{12}$−PTFEMA$_{98}$ spherical nanoparticles could be converted into a conversion vs time curve using the Beer−Lambert equation.[23] However, this approach assumes that there is no shift in λ_{max} for the trithiocarbonate absorption band at 446 nm, otherwise the implicit assumption that the molar extinction coefficient remains constant may not be valid. In this context, Skrabania et al. reported that dithiobenzoate-based RAFT agents are more sensitive to the nature of the reaction medium than trithiocarbonates, with a more polar environment typically leading to a blue shift in λ_{max}.[64] The λ_{max} vs time data recorded during the synthesis of PSMA$_{16}$−PTFEMA$_{86}$ spheres indicates a two-step 6 nm reduction in λ_{max} within the first 12 min of the TFEMA polymerization (see Figure S7). Moreover, a 6 nm difference was also observed for solutions of the CPDB RAFT agent in TFEMA and *n*-hexadecane (see Figure S8). Initially, we assumed that this blue shift in λ_{max} occurs at the onset of micellar nucleation, with diffusion of TFEMA monomer into the PTFEMA nanoparticle cores producing a more polar environment for the dithiobenzoate chain-ends. However, the kinetic data suggest that micellar nucleation only occurs after 1 h (see Figure 7b). Only 9% TFEMA conversion is achieved after a reaction time of 10 min, which corresponds to a PTFEMA DP of 8. Thus, only soluble PSMA$_{16}$−PTFEMA$_8$ oligomers are present at this time point. The λ_{max} values for molecularly-dissolved PSMA$_{16}$−PTFEMA$_9$ and PSMA$_{16}$−PTFEMA$_{19}$ copolymer chains prepared in *n*-hexadecane at 15% w/w solids were also determined at 90 °C (see Table S5). Since a 5−6 nm blue shift in λ_{max} was also observed for these latter two solutions, it is presumably related to the growing PTFEMA content of the copolymer chains. UV−visible spectra were initially recorded at a spectral resolution of ±3 nm, which accounts for the apparent two-step reduction in λ_{max}. Hence this in situ study was repeated using a higher spectral resolution of ±1 nm (see Figure 8). In this case, a more gradual reduction in λ_{max} from 515 to 507 nm was observed within 1.5 h (60% TFEMA conversion). Because of this significant shift in λ_{max}, the molar extinction coefficient for the corresponding absorption band cannot be assumed to remain constant throughout the polymerization. Thus, it would not be advisable to attempt to calculate monomer conversions from such spectroscopic data. In principle, the high transmittance observed for PSMA$_{16}$−PTFEMA$_{86}$ spheres prepared in *n*-hexadecane at 90 °C offers the opportunity to study the

kinetics of TFEMA polymerization via in situ visible absorption spectroscopy. However, in practice, the premature loss of dithiobenzoate chain-ends on the time scale of the polymerization and the significant blue shift in λ_{max} that is observed for such RAFT groups does not allow meaningful kinetic data to be obtained using this technique. In summary, our observations suggest that such in situ visible absorption spectroscopy experiments are best undertaken when using trithiocarbonate RAFT agents because the corresponding end-groups exhibit much better thermal stability and do not suffer from any discernible blue shift in the λ_{max} for their relatively weak visible absorption band.
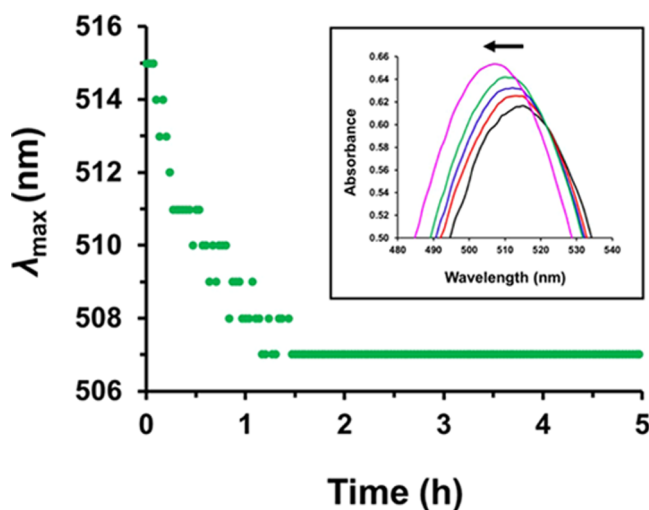

Figure 8. Systematic shift in λ_{max} observed for the relatively weak n → π* transition of the dithiobenzoate end-group during the synthesis of PSMA$_{16}$–PTFEMA$_{86}$ spherical nanoparticles via RAFT dispersion polymerization of TFEMA at 15% w/w solids in n-hexadecane at 90 °C. Inset: visible absorption spectra recorded for the reaction mixture after 4 min (black data), 8 min (red data), 14 min (blue data), 28 min (green data), and 90 min (purple data). Spectra were recorded every 2 min at a spectral resolution of ± 1 nm.

CONCLUSIONS

A series of PSMA$_9$–PTFEMA$_x$ diblock copolymer nano-objects (spheres, worms, or vesicles) can be prepared via RAFT dispersion polymerization of TFEMA at 90 °C in n-dodecane. When targeting PSMA$_9$–PTFEMA$_{200}$ vesicles, ^{19}F NMR spectroscopy studies indicated that more than 95% TFEMA conversion can be achieved within 5 h. Copolymer morphologies were assigned on the basis of TEM and DLS studies and confirmed by SAXS analysis. A pseudo-phase diagram was constructed to ensure the reproducible targeting of pure spheres, worms, and vesicles at 15−25% w/w solids. The first ever example of highly transparent block copolymer vesicles was obtained at 20 °C in n-dodecane; such vesicles can be prepared at up to 25% w/w solids. Similarly, transparent vesicles can be prepared in either n-tetradecane or n-hexadecane at 90 °C. In situ visible absorption spectroscopy studies conducted during the PISA synthesis of PSMA$_{16}$–PTFEMA$_{86}$ spheres in n-hexadecane revealed the premature loss of dithiobenzoate chain-ends at 90 °C. Unfortunately, this means that the kinetics of RAFT dispersion polymerization of TFEMA cannot be monitored using this technique. Nevertheless, these observations highlight the inferior thermal

stability of dithiobenzoate chain-ends compared to that of trithiocarbonate chain-ends. Finally, an 8 nm blue shift in λ_{max} is observed for the relatively weak n → π* transition exhibited by the dithiobenzoate chain-ends during the TFEMA polymerization relative to that of the dithiobenzoate-capped PSMA$_9$ precursor. This latter observation suggests that the problem of thermally labile RAFT chain-ends cannot be addressed by simply performing the TFEMA polymerization at a lower temperature.

ASSOCIATED CONTENT

Ⓢ Supporting Information

The Supporting Information is available free of charge at https://pubs.acs.org/doi/10.1021/acs.macromol.0c02646.

Assigned ^{19}F NMR spectrum, additional GPC traces, summary tables of copolymer characterization data, digital photographs of the visual appearance of PSMA$_9$−PTFEMA$_{63}$ worms, summary table of SAXS fitting parameters, transmittance vs wavelength plots recorded at various temperatures for a 25% w/w PSMA$_9$−PTFEMA$_{294}$ vesicle dispersion in n-dodecane, summary table of PSMA$_{16}$−PTFEMA$_{86}$ characterization data, TEM images of the PSMA$_{16}$−PTFEMA$_{86}$ spheres, absorption vs time data for the PSMA$_{16}$ stabilizer block recorded in n-hexadecane, digital photograph and visible absorption spectra of CPDB solutions prepared in n-hexadecane/TFEMA, additional λ_{max} vs time data for the synthesis of PSMA$_{16}$−PTFEMA$_{86}$ spheres, summary table of the λ_{max} data of the PSMA$_{16}$ stabilizer block and PSMA$_{16}$−PTFEMA$_x$ chains, and details of the three scattering models used for SAXS analysis (PDF)

AUTHOR INFORMATION

Corresponding Author

Steven P. Armes − *Dainton Building, Department of Chemistry, The University of Sheffield, Sheffield, South Yorkshire S3 7HF, U.K.;* ⓘ orcid.org/0000-0002-8289-6351; Email: s.p.armes@sheffield.ac.uk

Authors

Csilla György − *Dainton Building, Department of Chemistry, The University of Sheffield, Sheffield, South Yorkshire S3 7HF, U.K.*

Matthew J. Derry − *Dainton Building, Department of Chemistry, The University of Sheffield, Sheffield, South Yorkshire S3 7HF, U.K.;* ⓘ orcid.org/0000-0001-5010-6725

Erik J. Cornel − *Dainton Building, Department of Chemistry, The University of Sheffield, Sheffield, South Yorkshire S3 7HF, U.K.*

Complete contact information is available at:
https://pubs.acs.org/10.1021/acs.macromol.0c02646

Notes

The authors declare no competing financial interest.

■ REFERENCES

(1) Newman, S. Note on Colloidal Dispersions from Block Copolymers. *J. Appl. Polym. Sci.* 1962, 6, S15–S16.

(2) Krause, S. Dilute Solution Properties of a Styrene-Methyl Methacrylate Block Copolymer. *J. Phys. Chem. A* 1964, 68, 1948–1955.

(3) Tuzar, Z.; Kratochvíl, P. Block and Graft Copolymer Micelles in Solution. *Adv. Colloid Interface Sci.* 1976, 6, 201–232.

(4) Zhang, L.; Eisenberg, A. Multiple Morphologies of "Crew-Cut" Aggregates of Polystyrene-b-Poly(Acrylic Acid) Block Copolymers. *Science* 1995, 268, 1728–1731.

(5) Howse, J. R.; Jones, R. A. L.; Battaglia, G.; Ducker, R. E.; Leggett, G. J.; Ryan, A. J. Templated Formation of Giant Polymer Vesicles with Controlled Size Distributions. *Nat. Mater.* 2009, 8, 507–511.

(6) Charleux, B.; Delaittre, G.; Rieger, J.; D'Agosto, F. Polymerization-Induced Self-Assembly: From Soluble Macromolecules to Block Copolymer Nano-Objects in One Step. *Macromolecules* 2012, 45, 6753–6765.

(7) Monteiro, M. J.; Cunningham, M. F. Polymer Nanoparticles via Living Radical Polymerization in Aqueous Dispersions: Design and Applications. *Macromolecules* 2012, 45, 4939–4957.

(8) Sun, J. T.; Hong, C. Y.; Pan, C. Y. Formation of the Block Copolymer Aggregates via Polymerization-Induced Self-Assembly and Reorganization. *Soft Matter* 2012, 8, 7753–7767.

(9) Warren, N. J.; Armes, S. P. Polymerization-Induced Self-Assembly of Block Copolymer Nano-Objects via RAFT Aqueous Dispersion Polymerization. *J. Am. Chem. Soc.* 2014, 136, 10174–10185.

(10) Canning, S. L.; Smith, G. N.; Armes, S. P. A Critical Appraisal of RAFT-Mediated Polymerization-Induced Self-Assembly. *Macromolecules* 2016, 49, 1985–2001.

(11) Lowe, A. B. RAFT Alcoholic Dispersion Polymerization with Polymerization-Induced Self-Assembly. *Polymer* 2016, 106, 161–181.

(12) Derry, M. J.; Fielding, L. A.; Armes, S. P. Polymerization-Induced Self-Assembly of Block Copolymer Nanoparticles via RAFT Non-Aqueous Dispersion Polymerization. *Prog. Polym. Sci.* 2016, 52, 1–18.

(13) Yeow, J.; Boyer, C. Photoinitiated Polymerization-Induced Self-Assembly (Photo-PISA): New Insights and Opportunities. *Adv. Sci.* 2017, 4, No. 1700137.

(14) Penfold, N. J. W.; Yeow, J.; Boyer, C.; Armes, S. P. Emerging Trends in Polymerization-Induced Self-Assembly. *ACS Macro Lett.* 2019, 8, 1029–1054.

(15) D'Agosto, F.; Rieger, J.; Lansalot, M. RAFT-Mediated Polymerization-Induced Self-Assembly. *Angew. Chem., Int. Ed.* 2020, 59, 8368–8392.

(16) Cornel, E. J.; Jiang, J.; Chen, S.; Du, J. Principles and Characteristics of Polymerization-Induced Self-Assembly with Various Polymerization Techniques. *CCS Chem.* 2020, 2, 2104–2125.

(17) Semsarilar, M.; Jones, E. R.; Armes, S. P. Comparison of Pseudo-Living Character of RAFT Polymerizations Conducted under Homogeneous and Heterogeneous Conditions. *Polym. Chem.* 2014, 5, 195–203.

(18) Guo, L.; Jiang, Y.; Qiu, T.; Meng, Y.; Li, X. One-Pot Synthesis of Poly(Methacrylic Acid)-b-Poly(2,2,2-Trifluoroethyl Methacrylate) Diblock Copolymers via RAFT Polymerization. *Polymer* 2014, 55, 4601–4610.

(19) Akpinar, B.; Fielding, L. A.; Cunningham, V. J.; Ning, Y.; Mykhaylyk, O. O.; Fowler, P. W.; Armes, S. P. Determining the Effective Density and Stabilizer Layer Thickness of Sterically Stabilized Nanoparticles. *Macromolecules* 2016, 49, 5160–5171.

(20) Rymaruk, M. J.; Thompson, K. L.; Derry, M. J.; Warren, N. J.; Ratcliffe, L. P. D.; Williams, C. N.; Brown, S. L.; Armes, S. P. Bespoke Contrast-Matched Diblock Copolymer Nanoparticles Enable the Rational Design of Highly Transparent Pickering Double Emulsions. *Nanoscale* 2016, 8, 14497–14506.

(21) Thompson, K. L.; Cinotti, N.; Jones, E. R.; Mable, C. J.; Fowler, P. W.; Armes, S. P. Bespoke Diblock Copolymer Nanoparticles Enable the Production of Relatively Stable Oil-in-Water Pickering Nanoemulsions. *Langmuir* 2017, 33, 12616–12623.

(22) Chakrabarty, A.; Ponnupandian, S.; Kang, N. G.; Mays, J. W.; Singha, N. K. Designing Superhydrophobic Surface Based on Fluoropolymer–Silica Nanocomposite via RAFT-Mediated Polymerization-Induced Self-Assembly. *J. Polym. Sci. Part A Polym. Chem.* 2018, 56, 266–275.

(23) Cornel, E. J.; Meurs, S.; Van Smith, T.; Hora, P. S. O.; Armes, S. P. In Situ Spectroscopic Studies of Highly Transparent Nanoparticle Dispersions Enable Assessment of Trithiocarbonate Chain-End Fidelity during RAFT Dispersion Polymerization in Nonpolar Media. *J. Am. Chem. Soc.* 2018, 140, 12980–12988.

(24) Smith, G. N.; Derry, M. J.; Hallett, J. E.; Lovett, J. R.; Mykhaylyk, O. O.; Neal, T. J.; Prévost, S.; Armes, S. P. Refractive Index Matched, Nearly Hard Polymer Colloids. *Proc. R. Soc. A* 2019, 475, No. 20180763.

(25) Rymaruk, M. J.; Hunter, S. J.; O'Brien, C. T.; Brown, S. L.; Williams, C. N.; Armes, S. P. RAFT Dispersion Polymerization in Silicone Oil. *Macromolecules* 2019, 52, 2822–2832.

(26) Thompson, K. L.; Derry, M. J.; Hatton, F. L.; Armes, S. P. Long-Term Stability of n-Alkane-in-Water Pickering Nanoemulsions: Effect of Aqueous Solubility of Droplet Phase on Ostwald Ripening. *Langmuir* 2018, 34, 9289–9297.

(27) Docherty, P. J.; Girou, C.; Derry, M. J.; Armes, S. P. Epoxy-Functional Diblock Copolymer Spheres, Worms and Vesicles via Polymerization-Induced Self-Assembly in Mineral Oil. *Polym. Chem.* 2020, 11, 3332–3339.

(28) György, C.; Hunter, S. J.; Girou, C.; Derry, M. J.; Armes, S. P. Synthesis of Poly(Stearyl Methacrylate)-Poly(2-Hydroxypropyl Methacrylate) Diblock Copolymer Nanoparticles via RAFT Dispersion Polymerization of 2-Hydroxypropyl Methacrylate in Mineral Oil. *Polym. Chem.* 2020, 11, 4579–4590.

(29) Trent, J. S. Ruthenium Tetraoxide Staining of Polymers: New Preparative Methods for Electron Microscopy. *Macromolecules* 1984, 17, 2930–2931.

(30) Pauw, B. R.; Smith, A. J.; Snow, T.; Terrill, N. J.; Thünemann, A. F. The Modular Small-Angle X-Ray Scattering Data Correction Sequence. *J. Appl. Crystallogr.* 2017, 50, 1800–1811.

(31) Ilavsky, J.; Jemian, P. R. Irena: Tool Suite for Modeling and Analysis of Small-Angle Scattering. *J. Appl. Crystallogr.* 2009, 42, 347–353.

(32) Derry, M. J.; Fielding, L. A.; Warren, N. J.; Mable, C. J.; Smith, A. J.; Mykhaylyk, O. O.; Armes, S. P. In Situ Small-Angle X-Ray Scattering Studies of Sterically-Stabilized Diblock Copolymer Nanoparticles Formed during Polymerization-Induced Self-Assembly in Non-Polar Media. *Chem. Sci.* 2016, 7, 5078–5090.

(33) Blanazs, A.; Madsen, J.; Battaglia, G.; Ryan, A. J.; Armes, S. P. Mechanistic Insights for Block Copolymer Morphologies: How Do Worms Form Vesicles? *J. Am. Chem. Soc.* 2011, 133, 16581–16587.

(34) Docherty, P. J.; Derry, M. J.; Armes, S. P. RAFT Dispersion Polymerization of Glycidyl Methacrylate for the Synthesis of Epoxy-Functional Block Copolymer Nanoparticles in Mineral Oil. *Polym. Chem.* 2019, 10, 603–611.

(35) Derry, M. J.; Fielding, L. A.; Armes, S. P. Industrially-Relevant Polymerization-Induced Self-Assembly Formulations in Non-Polar Solvents: RAFT Dispersion Polymerization of Benzyl Methacrylate. *Polym. Chem.* 2015, 6, 3054–3062.

(36) Chiefari, J.; Chong, Y. K. B.; Ercole, F.; Krstina, J.; Jeffery, J.; Le, T. P. T.; Mayadunne, R. T. A.; Meijs, G. F.; Moad, C. L.; Moad, G.; Rizzardo, E.; Thang, S. H. Living Free-Radical Polymerization by

Reversible Addition-Fragmentation Chain Transfer: The RAFT Process. *Macromolecules* **1998**, *31*, 5559−5562.

(37) Moad, G.; Rizzardo, E.; Thang, S. H. Living Radical Polymerization by the RAFT Process. *Aust. J. Chem.* **2005**, *58*, 379−410.

(38) Moad, G.; Rizzardo, E.; Thang, S. H. Radical Addition-Fragmentation Chemistry in Polymer Synthesis. *Polymer* **2008**, *49*, 1079−1131.

(39) Heatley, F.; Lovell, P. A.; Yamashita, T. Chain Transfer to Polymer in Free-Radical Solution Polymerization of 2-Ethylhexyl Acrylate Studied by NMR Spectroscopy. *Macromolecules* **2001**, *34*, 7636−7641.

(40) Blanazs, A.; Verber, R.; Mykhaylyk, O. O.; Ryan, A. J.; Heath, J. Z.; Douglas, C. W. I.; Armes, S. P. Sterilizable Gels from Thermoresponsive Block Copolymer Worms. *J. Am. Chem. Soc.* **2012**, *134*, 9741−9748.

(41) Verber, R.; Blanazs, A.; Armes, S. P. Rheological Studies of Thermo-Responsive Diblock Copolymer Worm Gels. *Soft Matter* **2012**, *8*, 9915−9922.

(42) Warren, N. J.; Mykhaylyk, O. O.; Mahmood, D.; Ryan, A. J.; Armes, S. P. RAFT Aqueous Dispersion Polymerization Yields Poly(Ethylene Glycol)-Based Diblock Copolymer Nano-Objects with Predictable Single Phase Morphologies. *J. Am. Chem. Soc.* **2014**, *136*, 1023−1033.

(43) Penfold, N. J. W.; Lovett, J. R.; Warren, N. J.; Verstraete, P.; Smets, J.; Armes, S. P. PH-Responsive Non-Ionic Diblock Copolymers: Protonation of a Morpholine End-Group Induces an Order−Order Transition. *Polym. Chem.* **2016**, *7*, 79−88.

(44) Fielding, L. A.; Lane, J. A.; Derry, M. J.; Mykhaylyk, O. O.; Armes, S. P. Thermo-Responsive Diblock Copolymer Worm Gels in Non-Polar Solvents. *J. Am. Chem. Soc.* **2014**, *136*, 5790−5798.

(45) Pei, Y.; Thurairajah, L.; Sugita, O. R.; Lowe, A. B. RAFT Dispersion Polymerization in Nonpolar Media: Polymerization of 3-Phenylpropyl Methacrylate in N-Tetradecane with Poly(Stearyl Methacrylate) Homopolymers as Macro Chain Transfer Agents. *Macromolecules* **2015**, *48*, 236−244.

(46) Lovett, J. R.; Warren, N. J.; Armes, S. P.; Smallridge, M. J.; Cracknell, R. B. Order-Order Morphological Transitions for Dual Stimulus Responsive Diblock Copolymer Vesicles. *Macromolecules* **2016**, *49*, 1016−1025.

(47) Deng, R.; Ning, Y.; Jones, E. R.; Cunningham, V. J.; Penfold, N. J. W.; Armes, S. P. Stimulus-Responsive Block Copolymer Nano-Objects and Hydrogels: Via Dynamic Covalent Chemistry. *Polym. Chem.* **2017**, *8*, 5374−5380.

(48) Jesson, C. P.; Pearce, C. M.; Simon, H.; Werner, A.; Cunningham, V. J.; Lovett, J. R.; Smallridge, M. J.; Warren, N. J.; Armes, S. P. H2O2 Enables Convenient Removal of RAFT End-Groups from Block Copolymer Nano-Objects Prepared via Polymerization-Induced Self-Assembly in Water. *Macromolecules* **2017**, *50*, 182−191.

(49) Le, D.; Wagner, F.; Takamiya, M.; Hsiao, I. L.; Gil Alvaradejo, G.; Strähle, U.; Weiss, C.; Delaittre, G. Straightforward Access to Biocompatible Poly(2-Oxazoline)-Coated Nanomaterials by Polymerization-Induced Self-Assembly. *Chem. Commun.* **2019**, *55*, 3741−3744.

(50) Pham, B. T. T.; Nguyen, D.; Huynh, V. T.; Pan, E. H.; Shirodkar-Robinson, B.; Carey, M.; Serelis, A. K.; Warr, G. G.; Davey, T.; Such, C. H.; Hawkett, B. S. Aqueous Polymeric Hollow Particles as an Opacifier by Emulsion Polymerization Using Macro-RAFT Amphiphiles. *Langmuir* **2018**, *34*, 4255−4263.

(51) Pedersen, J. S. Form Factors of Block Copolymer Micelles with Spherical, Ellipsoidal and Cylindrical Cores. *J. Appl. Crystallogr.* **2000**, *33*, 637−640.

(52) Bang, J.; Jain, S.; Li, Z.; Lodge, T. P.; Pedersen, J. S.; Kesselman, E.; Talmon, Y. Sphere, Cylinder, and Vesicle Nano-aggregates in Poly(Styrene-b-Isoprene) Diblock Copolymer Solutions. *Macromolecules* **2006**, *39*, 1199−1208.

(53) Warren, N. J.; Mykhaylyk, O. O.; Ryan, A. J.; Williams, M.; Doussineau, T.; Dugourd, P.; Antoine, R.; Portale, G.; Armes, S. P. Testing the Vesicular Morphology to Destruction: Birth and Death of Diblock Copolymer Vesicles Prepared via Polymerization-Induced Self-Assembly. *J. Am. Chem. Soc.* **2015**, *137*, 1929−1937.

(54) Kwak, Y.; Goto, A.; Tsujii, Y.; Murata, Y.; Komatsu, K.; Fukuda, T. A Kinetic Study on the Rate Retardation in Radical Polymerization of Styrene with Addition-Fragmentation Chain Transfer. *Macromolecules* **2002**, *35*, 3026−3029.

(55) Moad, G.; Rizzardo, E.; Thang, S. H. End-Functional Polymers, Thiocarbonylthio Group Removal/Transformation and Reversible Addition-Fragmentation-Chain Transfer (RAFT) Polymerization. *Polym. Int.* **2011**, *60*, 9−25.

(56) Willcock, H.; O'Reilly, R. K. End Group Removal and Modification of RAFT Polymers. *Polym. Chem.* **2010**, *1*, 149−157.

(57) Moad, G.; Chong, Y. K.; Postma, A.; Rizzardo, E.; Thang, S. H. Advances in RAFT Polymerization: The Synthesis of Polymers with Defined End-Groups. *Polymer* **2005**, *46*, 8458−8468.

(58) Postma, A.; Davis, T. P.; Moad, G.; O'Shea, M. S. Thermolysis of RAFT-Synthesized Polymers. A Convenient Method for Trithiocarbonate Group Elimination. *Macromolecules* **2005**, *38*, 5371−5374.

(59) Postma, A.; Davis, T. P.; Li, G.; Moad, G.; O'Shea, M. S. RAFT Polymerization with Phthalimidomethyl Trithiocarbonates or Xanthates. On the Origin of Bimodal Molecular Weight Distributions in Living Radical Polymerization. *Macromolecules* **2006**, *39*, 5307−5318.

(60) Liu, Y.; He, J.; Xu, J.; Fan, D.; Tang, W.; Yang, Y. Thermal Decomposition of Cumyl Dithiobenzoate. *Macromolecules* **2005**, *38*, 10332−10335.

(61) Xu, J.; He, J.; Fan, D.; Tang, W.; Yang, Y. Thermal Decomposition of Dithioesters and Its Effect on RAFT Polymerization. *Macromolecules* **2006**, *39*, 3753−3759.

(62) Hosseini Nejad, E.; Castignolles, P.; Gilbert, R. G.; Guillaneuf, Y. Synthesis of Methacrylate Derivatives Oligomers by Dithiobenzoate-RAFT-mediated Polymerization. *J. Polym. Sci., Part A: Polym. Chem.* **2008**, *46*, 2277−2289.

(63) Zhou, Y.; He, J.; Li, C.; Hong, L.; Yang, Y. Dependence of Thermal Stability on Molecular Structure of RAFT/MADIX Agents: A Kinetic and Mechanistic Study. *Macromolecules* **2011**, *44*, 8446−8457.

(64) Skrabania, K.; Miasnikova, A.; Bivigou-Koumba, A. M.; Zehm, D.; Laschewsky, A. Examining the UV-Vis Absorption of RAFT Chain Transfer Agents and Their Use for Polymer Analysis. *Polym. Chem.* **2011**, *2*, 2074−2083.